

# Million-scale Object Detection with Large Vision Model

Feng Lin<sup>1,2</sup>, Wenze Hu<sup>1</sup>, Yaowei Wang<sup>3</sup>, Yonghong Tian<sup>3</sup>, Guangming Lu<sup>2</sup>, Fanglin Chen<sup>2</sup>, Yong Xu<sup>4</sup> and Xiaoyu Wang<sup>1\*</sup>

<sup>1</sup>Intellifusion Inc., Shenzhen, China .

<sup>2</sup>Harbin Institute of Technology, Shenzhen, China .

<sup>3</sup>Peng Cheng Laboratory, Shenzhen, China .

<sup>4</sup>South China University of Technology, Guangzhou, China.

\*Corresponding author(s). E-mail(s): [fanghuaxue@gmail.com](mailto:fanghuaxue@gmail.com);

Contributing authors: [lin1993@mail.ustc.edu.cn](mailto:lin1993@mail.ustc.edu.cn); [windsor.hwu@gmail.com](mailto:windsor.hwu@gmail.com);  
[wangyw@pcl.ac.cn](mailto:wangyw@pcl.ac.cn); [yhtian@pku.edu.cn](mailto:yhtian@pku.edu.cn); [luguangm@hit.edu.cn](mailto:luguangm@hit.edu.cn); [chenfanglin@hit.edu.cn](mailto:chenfanglin@hit.edu.cn);  
[yxu@scut.edu.cn](mailto:yxu@scut.edu.cn);

## Abstract

Over the past few years, there has been growing interest in developing a broad, universal, and general-purpose computer vision system. Such a system would have the potential to solve a wide range of vision tasks simultaneously, without being restricted to a specific problem or data domain. This is crucial for practical, real-world computer vision applications. In this study, we focus on the million-scale multi-domain universal object detection problem, which presents several challenges, including cross-dataset category label duplication, label conflicts, and the need to handle hierarchical taxonomies. Furthermore, there is an ongoing challenge in the field to find a resource-efficient way to leverage large pre-trained vision models for million-scale cross-dataset object detection. To address these challenges, we introduce our approach to label handling, hierarchy-aware loss design, and resource-efficient model training using a pre-trained large model. Our method was ranked *second* in the object detection track of the Robust Vision Challenge 2022 (RVC 2022). We hope that our detailed study will serve as a useful reference and alternative approach for similar problems in the computer vision community. The code is available at <https://github.com/linfeng93/Large-UniDet>.

**Keywords:** universal object detection, large vision model, resource-efficient, hierarchical taxonomy

## 1 Introduction

A universal, general-purpose computer vision system has become a trend in the development of computer vision technology (Gong, Dai, Chen, Li, & Van Gool, 2021; Hasan, Liao, Li, Akram, & Shao, 2021; Y. He et al., 2022; Wang, Cai, Gao, & Vasconcelos, 2019; X. Zhou, Koltun, & Krähenbühl, 2022). This universal vision model is a multi-talented agent that can simultaneously

solve a wide range of vision tasks with minimal human intervention. Researchers no longer need to train separate models for each individual vision task or fine-tune an existing model for a specific data domain. Instead, they can achieve all tasks with a single effort. The universality of this model is a promising direction towards human-like AI and has important implications for real-world computer vision applications (Yuan et al., 2021).

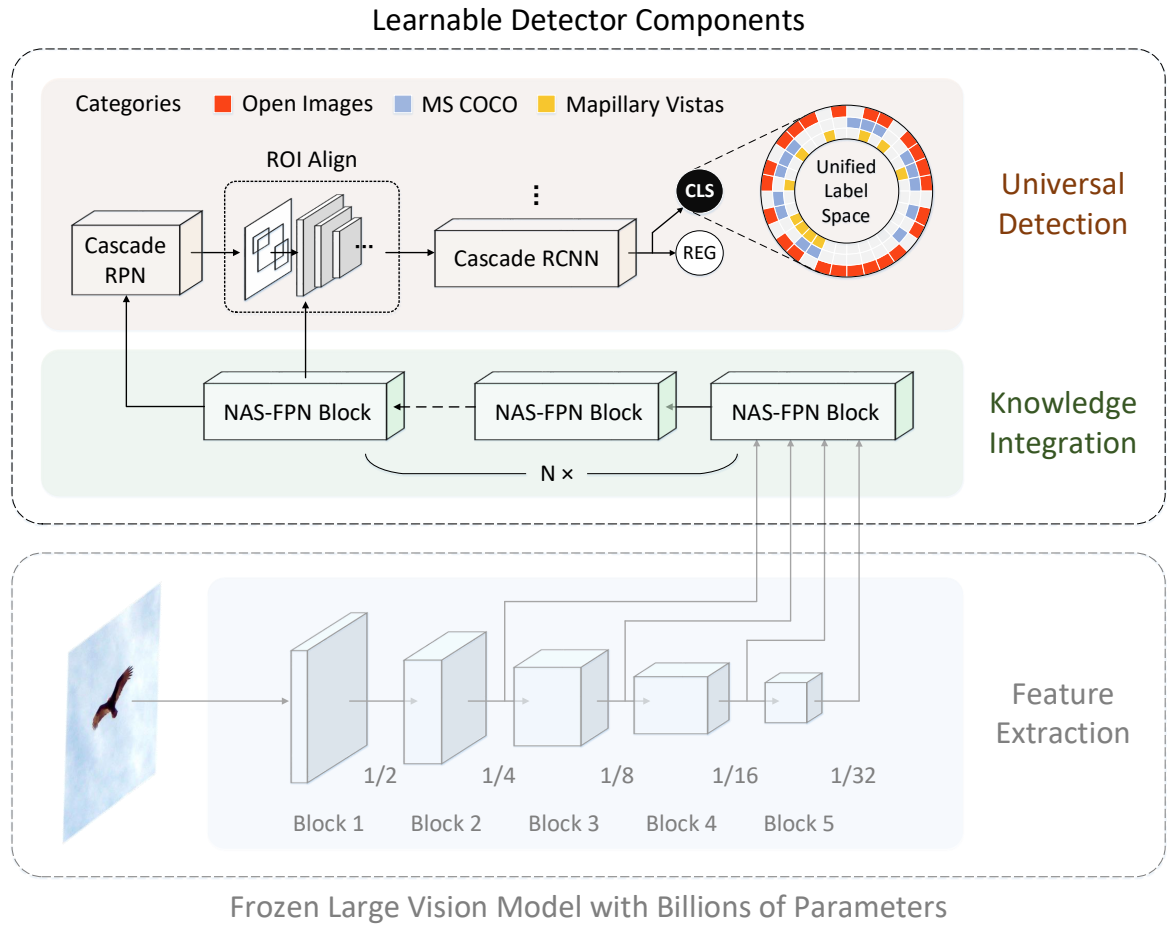


**Fig. 1** Overview. The design of Large-UniDet is based on a two-stage RCNN-style object detection network. The frozen backbone is a RegNet architecture initialized with the weights of SEER models. The NAS-FPN blocks can be stacked  $N$  times for a better accuracy-cost trade-off. The classification branch of Cascade R-CNN outputs 541 class scores including the *background* as the cardinality of the unified label space is 540.

In this study, we aim to contribute to the development of universal vision technology. Specifically, we focus on the million-scale universal object detection problem across different domains. The goal is to have a single object detector that can perform the inference process once and generate unified detection results across all datasets, regardless of their differences.

The challenge of developing a million-scale multi-domain universal object detection system lies in two areas: (a) curating a large-scale and diverse training dataset, and (b) creating a robust visual representation approach. The training dataset must cover a wide range of data domains in order to achieve satisfactory results

across domains. However, such a dataset is currently not available. Furthermore, building a unified large-scale dataset with dense annotations for object detection (Zhao et al., 2020; X. Zhou et al., 2022) and similar fine-grained computer vision tasks (Bevandić & Šegvić, 2022; Lambert, Liu, Sener, Hays, & Koltun, 2020; Ranftl, Lasinger, Hafner, Schindler, & Koltun, 2020) is cost-prohibitive. In terms of robust visual representations, it is challenging to ensure the common object detector is robust to the million-scale and diverse source data, as objects of interest can vary greatly in different images.

Fortunately, with the growing number of available detection datasets, researchers can now implement universal object detectors by reusing

these datasets. We take advantage of these datasets by unifying their independent label spaces, allowing us to handle multi-domain object detection with different label vocabularies. However, using multiple diverse datasets can result in annotation inconsistencies, such as label duplication, conflicts, and incomplete hierarchical taxonomy. To address these issues, we have designed a comprehensive loss formulation in the unified label space.

To tackle the robustness issue for the million-scale multi-domain object detection problem, we utilize large pre-trained vision models. Recent studies have demonstrated the superiority of larger models in capturing higher-quality visual representations compared to smaller models (Bello et al., 2021; Kolesnikov, Zhai, & Beyer, 2019; Radosavovic, Kosaraju, Girshick, He, & Dollár, 2020). These high-quality representations lead to better generalization both in-domain and out-of-domain (Goyal et al., 2022). Thus, we believe that the use of large well-trained vision models would significantly improve the performance of universal object detection for million-scale diverse datasets. Our experiments indeed show a noticeable improvement in performance by using larger vision models in the universal object detection task.

As we acquire the feature robustness by taking advantage of large pre-trained vision models, computational resources become a critical demand because of both computational and memory-wise costs. Without many computational resources yet, we introduce a resource-efficient training formulation for large vision models inspired by a recent work (Vasconcelos, Birodkar, & Dumoulin, 2022), which saves considerable computational resources, especially GPU memory, during the training procedures.

This paper discusses our approach to the challenge of multi-domain universal object detection at a scale of millions of diverse datasets. We utilize the power of large pre-trained vision models and present an efficient training formulation that saves computational resources. Our method, Large-UniDet, has achieved remarkable results and won the second prize in the object detection track of the Robust Vision Challenge

2022<sup>1</sup>. The success of our approach is attributed to the efficient formulation design, careful label handling, and knowledge transfer from large-scale pre-training.

Our contributions are summarized as follows.

- Our approach explores the use of large vision models for the challenging task of million-scale multi-domain universal object detection.
- We present a resource-efficient training formulation for large vision models in universal object detection, which saves computational resources during training procedures.
- With the unified label space, we handle multi-domain object detection with different label vocabularies and overcome cross-dataset label duplication and semantic hierarchy problems.
- The proposed method, Large-UniDet, achieved the 2nd prize in the object detection track of RVC 2022, demonstrating its impressive performance and robustness.

## 2 Related Works

### 2.1 Universal Object Detector

Recent years have seen a growing interest in universal object detection. Wang et al. (Wang et al., 2019) propose a universal detector with a domain attention module that leverages shared knowledge across different data domains. The design consists of multiple dataset-specific detectors that share most network parameters while keeping the categories of each dataset separate. Universal-RCNN (Xu, Fang, Liang, Kang, & Li, 2020), on the other hand, tries to incorporate graph transfer learning to model the intra-domain and inter-domain semantics of categories from multiple datasets (Krishna et al., 2017; T.-Y. Lin et al., 2014; B. Zhou et al., 2017). Unlike these methods, Zhao et al. (Zhao et al., 2020) build a unified label space by manually merging multiple label spaces of different datasets, and their framework is dedicated to managing partial annotations through the use of pseudo-labeling. UniDet (X. Zhou et al., 2022), in contrast, presents an automatic method to unify label spaces based on visual concepts generated by a partitioned object detector with three separate branches. Cai et al. (L. Cai et al., 2022)

---

<sup>1</sup>[www.robustvision.net/leaderboard.php?benchmark=object](http://www.robustvision.net/leaderboard.php?benchmark=object), IFFF\_RVC entry on Leaderboard

construct a unified label space by extracting category embeddings from each dataset using a language model. Recently, Meng et al. (Meng et al., 2022) leveraged pre-trained language embeddings to generate adapted queries for each category embedding across different datasets, modeling object classification as a region-word alignment problem without a merged label space.

Similar to the methods mentioned above based on the unified label spaces, we propose a solution to improve the unified label space in universal object detection by modifying the manually-crafted taxonomy used in the RVC challenge. Our proposed method also addresses the challenges posed by label duplication and semantic hierarchy issues across multiple datasets.

## 2.2 Pre-training for Vision Tasks

Pre-training is a widespread technique in computer vision (Azizi et al., 2021; L. Cai et al., 2022; Caron et al., 2020; Joulin, Maaten, Jabri, & Vasilache, 2016; Kornblith, Shlens, & Le, 2019; Sun, Shrivastava, Singh, & Gupta, 2017) that enhances performance by using backbone models trained on large-scale datasets such as ImageNet (Deng et al., 2009), JFT-300M (Sun et al., 2017), Open-Images (Kuznetsova et al., 2020), or web-collected data (Goyal et al., 2022). The backbone generates robust visual representations that can benefit various downstream vision tasks (Goyal et al., 2022). For object detection, the choice of the pre-trained backbone is crucial for determining performance (Y. Liu et al., 2020). Typically, the strength of a pre-trained backbone comes from its (a) powerful architecture, (b) broad training data, and (c) sophisticated pre-training methods.

*Stronger architecture.* To better understand the impact of backbone architectures on object detection performance, Huang et al. (Huang et al., 2017) studied the relationship between backbone capacities and performance. Liu et al. (Y. Liu et al., 2020) took a different approach and improved the backbone’s strength by combining multiple identical backbones. Furthermore, Liu et al. (Z. Liu et al., 2022) leveraged the power of vision transformers to create an extremely large object detector by using an expanded Swin transformer as the feature extractor. While many works in the field aim to improve performance through

innovative model design, space constraints prevent further listing of related literature.

*Training data.* In terms of the training data, Sun et al. (Sun et al., 2017) have demonstrated the impact of using a large-scale dataset JFT-300M on the robustness of representation learning. Bu et al. (Bu, Peng, Yan, Tan, & Zhang, 2021) have taken a different approach by combining various detection datasets (Dollar, Wojek, Schiele, & Perona, 2011; Kuznetsova et al., 2020; T.-Y. Lin et al., 2014; S. Shao et al., 2019; Zhang, Benenson, & Schiele, 2017) to attain better pre-trained weights for transfer learning in downstream tasks. Meanwhile, Cai et al. (L. Cai et al., 2022) have utilized existing detection datasets (Gupta, Dollar, & Girshick, 2019; Kuznetsova et al., 2020; S. Shao et al., 2019) to create a large pre-training dataset through careful curation based on well-defined principles. It should be noted that due to space constraints, additional related works are not discussed here.

*Pre-training approach.* The recent advancements in model pre-training (Caron et al., 2020; K. He et al., 2022; K. He, Fan, Wu, Xie, & Girshick, 2020; F. Lin, Xu, Li, Xiong, & Qi, 2021; Xu et al., 2022) have demonstrated the superiority of self-supervised methods over supervised approaches in computer vision tasks, such as object detection, semantic segmentation, and image classification. With the advantage of utilizing unlimited diverse image data from the web, self-supervised pre-training methods are capable of capturing more discriminative visual representations without relying on manual annotations (Goyal et al., 2022). Furthermore, the training of vision foundation models on large-scale image-text data (Jia et al., 2021; Radford et al., 2021; J. Shao et al., 2021; Yuan et al., 2021) highlights the significant impact of representation learning on both in-domain and out-of-domain downstream tasks.

To enhance the performance of our universal object detector, we have chosen to use large self-supervised vision models known as SEER models (Goyal et al., 2022) as the backbone. As discussed earlier, robust backbones can be attributed to high-capacity architectures, a diverse training data, and cutting-edge pre-training techniques. The largest SEER model that we will be using boasts a massive 10 billion network parameters. The SEER models are trained on a self-supervised

clustering-based method (Caron et al., 2020) utilizing 1 billion less biased uncured images collected from the web. This results in robust visual representations that perform well on both in-domain and out-of-domain benchmarks (Goyal et al., 2022). Our belief is that the SEER backbones will be capable of producing more discriminative features and provide better out-of-distribution generalization for the task of universal object detection across datasets with varying characteristics.

## 3 Method

### 3.1 Resource-efficient Detection with a Large Vision Model

In this section, we introduce our strong object detector that is built on large pre-trained backbone networks. The use of large vision models has been demonstrated to improve the performance of many computer vision tasks. However, the enormous computational and memory requirements for training these models limit their practical use (Dai, Liu, Le, & Tan, 2021; Radford et al., 2021; J. Shao et al., 2021). To address this challenge, we propose a computationally & memory efficient training approach that freezes the parameters of the billions of pre-trained backbone neurons and fine-tunes the extracted visual representations on the subsequent detector components. This allows us to train our largest model on a limited number of GPUs, specifically 16 NVIDIA 3090 GPUs. Our resource-efficient approach leverages the recent advancements in knowledge transfer (Vasconcelos et al., 2022) and is specifically designed for large pre-trained vision models, providing a valuable resource for the computer vision community that is interested in object detection with limited computational resources.

Fig. 1 illustrates the overall framework. Each detector component is described in detail in the remaining content of this section.

#### 3.1.1 Frozen Backbone with Billions of Parameters

In view of the superior performance of the SEER model (Goyal et al., 2022) in terms of fairness and bias reduction across different domains, we have

adopted it as the backbone of our object detection network to ensure robust visual representations across three distinct datasets: MS COCO (COCO), OpenImages Dataset (OID), and Mapillary Vistas Dataset (MVD). Typically, to optimize object detectors, both the initialized backbone and subsequent detector components are fine-tuned on detection datasets. However, fine-tuning the backbone on smaller detection datasets can result in the backbone parameters drifting away from their pre-trained initialization, which can negatively impact detection performance (Vasconcelos et al., 2022). Additionally, fine-tuning a heavy backbone can significantly increase computational complexity. To achieve superior detection performance while managing computational complexity, we have chosen to freeze the backbone parameters during the training process. This efficient formulation not only saves resources but also positively impacts the performance of long-tailed object categories through knowledge preservation (Vasconcelos et al., 2022), which is important in the RVC multi-domain scenario.

With billions of uncured internet images, the SEER models are trained to achieve both in-domain and out-of-domain generalization. Based on the observation that the generalization increases with the model size (Goyal et al., 2022), we carefully evaluate the trade-off between cost and performance to determine the best version for our experiments and final submission for the RVC competition. In the end, we opt to use both the lighter version (SEER-RegNet32gf) and the second largest version (SEER-RegNet256gf) for our extensive evaluations.

#### 3.1.2 Cascade Detection Heads

In order to enhance the performance of our object detector, we implemented a two-stage RCNN-style detection framework with a frozen SEER backbone. Initial experiments using Faster RCNN (Ren, He, Girshick, & Sun, 2015) did not produce satisfactory results, likely due to its limited number of learnable parameters making it difficult to handle the large-scale detection tasks across diverse datasets. Taking inspiration from recent advances in the field (Vasconcelos et al., 2022), we adopted high-capacity Cascade



R-CNN (Z. Cai & Vasconcelos, 2018) as our detection heads, which greatly improved performance as discussed in Section 4.5.1.

### 3.1.3 Stacked Dense Neck

The Feature Pyramid Network (FPN) is a fundamental component in object detection frameworks, serving as an adaptive module that integrates and improves hierarchical features. It acts like a neck that connects the backbone and the subsequent detection heads. The original FPN design (T.-Y. Lin et al., 2017) transfers multi-level semantic information from the backbone through a top-down pathway and lateral connections, creating a simple and straightforward path for knowledge integration. Subsequent designs (Ghiasi, Lin, & Le, 2019; S. Liu, Qi, Qin, Shi, & Jia, 2018; Pang et al., 2019; Tan, Pang, & Le, 2020) have introduced cross-scale connections to reinforce visual representations with semantically important information and low-level details.

We employ a stacked, densely connected FPN, namely NAS-FPN (Ghiasi et al., 2019), as the neck of our object detector for the following four reasons.

- As universal object detection is to detect hundreds of object categories from various datasets, the impressive ability of NAS-FPN to generate robust representations meets the challenges of million-scale multi-domain detection.
- As we freeze the backbone, the remaining detector components require higher model capacity (described in Section 3.1.2), while stacked NAS-FPN offers excellent flexibility in constructing rich neck architecture.
- The released SEER models are trained on billions of uncurated web-scale images. Inevitably, there is some domain gap between the upstream pre-training dataset and downstream detection datasets. As we do not finetune the SEER models on the downstream data, we believe the early NAS-FPN blocks can act as domain adaptors to align the domain gap.
- Last but not least, we observe that multi-level side-outputs of SEER models have very different characteristics. Some shallow side-outputs are dense, while the deeper ones are generally sparse and weak. The rich connections of NAS-FPN offer more possible ways for better feature integration.

### 3.1.4 Adaptive RPN

In the context of multi-domain object detection, objects belonging to the same category can exhibit different characteristics across different domains. For example, a *person* in an autonomous driving dataset such as MVD is typically much smaller in the high-resolution street scenes, while a *person* in COCO images is usually much larger. This variation in object size highlights the need for an adaptive region proposal network (RPN) to generate high-quality proposals that can handle the diverse object sizes in each domain. The Cascade RPN (Vu, Jang, Pham, & Yoo, 2019) overcomes the limitations of traditional RPNs, which rely on heuristically determining appropriate scales and aspect ratios for pre-defined anchors. Additionally, having too many pre-defined anchors can slow down the training process. By incorporating the Cascade RPN into our network, we are able to improve the quality of proposals and increase the overall model capacity, providing the best of both worlds.

## 3.2 Cross-dataset Model Training

### 3.2.1 Label Space Unification Across Multiple Datasets

The goal of this section is to outline the creation of a unified label space for three datasets, addressing the issues of label duplication and semantic hierarchy across the datasets. The RVC organizers have provided a manually-crafted taxonomy<sup>2</sup> as a starting point. This taxonomy maps each category from COCO or MVD to a single category in the RVC official label space, as well as each leaf-node category from OID. However, the non-leaf categories from OID are not included in this label space. To complete the label space, we modify the official taxonomy by simply adding all of the non-leaf categories from OID, excluding the root entry. This results in a unified label space with a cardinality of 540.

The OID has a semantic hierarchy where the superclasses, or non-leaf categories, are considered to be more general than other classes. However, this leads to inconsistencies in granularity and results in issues such as label duplication and

---

<sup>2</sup>[https://github.com/ozendelait/rvc\\_devkit/blob/master/objdet/obj\\_det\\_mapping.csv](https://github.com/ozendelait/rvc_devkit/blob/master/objdet/obj_det_mapping.csv)

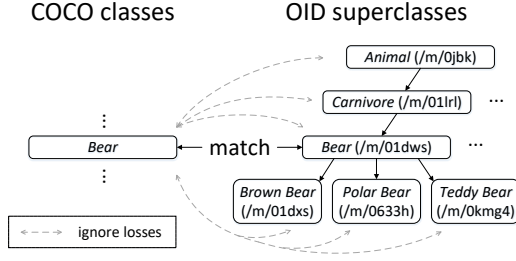


**Fig. 2** An example shows the loss suppression for semantically label duplication between COCO and OID.

problems with the semantic hierarchy. For example, the *person* (/m/01g317) superclass in OID and the *person* class in COCO are semantically the same, but are treated as separate categories. For another example, the *cow* class in COCO is semantically a child of the *animal* (/m/0jbjk) superclass in OID, but OID's hierarchy does not reflect this parent-child relationship. This overlap in taxonomy can negatively impact the performance of universal object detection. To address these issues, we propose a unified hierarchical taxonomy and implement a hierarchy-aware loss suppression method, which will be explained in Section 3.2.2 and 3.2.3, respectively.

### 3.2.2 Multi-label with Hierarchical Taxonomy Completion

To address the semantic hierarchy challenges in OID, we introduce a method of completing the

Two categories match in semantics	
COCO classes	OID superclasses
<i>sports ball</i>	<i>ball</i> (/m/018xm)
<i>bear</i>	<i>bear</i> (/m/01dws)
<i>bed</i>	<i>bed</i> (/m/03ssj5)
<i>bird</i>	<i>bird</i> (/m/015p6)
<i>boat</i>	<i>boat</i> (/m/019jd)
<i>car</i>	<i>car</i> (/m/0k4j)
<i>clock</i>	<i>clock</i> (/m/01x3z)
<i>person</i>	<i>person</i> (/m/01g317)
MVD classes	OID superclasses
<i>object-vehicle-car</i>	<i>car</i> (/m/0k4j)
<i>human-person</i>	<i>person</i> (/m/01g317)

**Table 1** The duplicated category names between OID superclasses and COCO / MVD classes in semantics.

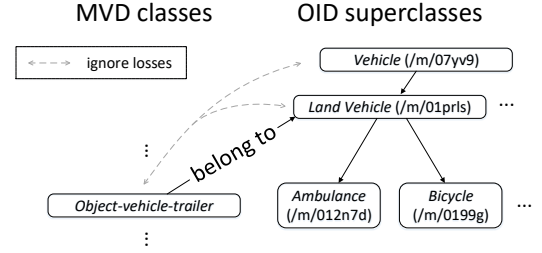


**Fig. 3** An example shows the loss suppression for semantic hierarchy between MVD and OID.

hierarchical taxonomy by incorporating categories from the RVC official taxonomy. The resolution of the remaining cross-dataset semantic hierarchy issues is presented in Section 3.2.3.

We convert the one-hot category labels to multi-class labels by considering all parent categories as positives for OID images. This is similar to UniDet (X. Zhou et al., 2022) but with the added consideration of the semantic hierarchies of COCO and MVD using the OID semantic hierarchy. For each annotated box that has been merged with an OID leaf-node category according to the RVC official taxonomy, we treat it as its OID equivalent. For instance, if the COCO *banana* and

The left as a descendant of the right in semantics	
COCO classes	OID superclasses
<i>cow</i>	<i>animal</i> (/m/0jbjk)
MVD classes	OID superclasses
<i>animal-ground</i>	<i>animal</i> (/m/0jbjk)
<i>-animal</i>	
<i>object-vehicle</i>	<i>land vehicle</i> (/m/01prls)
<i>-caravan</i>	
<i>object-vehicle-other</i>	<i>land vehicle</i> (/m/01prls)
<i>-vehicle</i>	
<i>object-vehicle-trailer</i>	<i>land vehicle</i> (/m/01prls)
<i>object-vehicle</i>	<i>land vehicle</i> (/m/01prls)
<i>-wheeled-slow</i>	
<i>object-support-traffic</i>	<i>traffic sign</i> (/m/01mqdt)
<i>-sign-frame</i>	
<i>object-traffic-sign</i>	<i>traffic sign</i> (/m/01mqdt)
<i>-back</i>	
<i>object-traffic-sign</i>	<i>traffic sign</i> (/m/01mqdt)
<i>-front</i>	

**Table 2** The parent-child category names between OID superclasses and COCO / MVD classes in semantics.

$$L_{rpn} = \frac{1}{N} \sum_{i=0}^N \sum_{s=0}^{S_{rpn}} (\alpha \cdot (1 - IoU(p_s^i, y_{rloc}^i)) + BCE(q_s^i, y_{rcls}^i)) \quad (1)$$

$$L_{head} = \frac{1}{N} \sum_{i=0}^N \sum_{s=0}^{S_{head}} (\beta \cdot SmoothL_1(r_s^i, y_{loc}^i) + \frac{\gamma}{C} \cdot \sum_{c=0}^C L_{cls}^c) \quad (2)$$

$$L_{cls}^c = (1 - \mathbb{1}_{\mathbb{D}(y_{cls}^i)}(c)) \cdot BCE(x_s^{ic}, \mathbb{1}_{\mathbb{P}(y_{cls}^i)}(c)) \quad (3)$$

the OID *banana* (/m/09qck) have been merged into a single mutual category, a bounding box annotated as *banana* from COCO would receive a positive label for the *fruit* category since *banana* belongs to the *fruit* superclass according to the OID semantic hierarchy. We employ a multi-label classifier in the detection heads and use *sigmoid* activation functions to obtain class confidence scores for each bounding box.

It is important to note that this hierarchical taxonomy completion is not a complete solution. There are several annotated objects from COCO and MVD that do not match any OID leaf-node category but are semantically associated with a certain superclass from OID. Instead of activating the corresponding parent categories, we handle these semantic hierarchies through an intricate adaptation in the loss function, which is discussed in the following section.

### 3.2.3 Hierarchy-aware Cross-dataset Loss Suppression

To address both label duplication and unsolved semantic hierarchies described in Sections 3.2.1 and 3.2.2, we propose a loss adaptation strategy called Hierarchy-Aware Cross-Dataset Loss Suppression (HCLS). This strategy is based on the semantic hierarchy of OID and suppresses losses over categories involved in label duplication and semantic hierarchy between OID and COCO/MVD in the box classification branches. More specifically,

- For each category from OID, HCLS ignores the losses over all its child categories, as a common practice for hierarchical taxonomy (Kuznetsova et al., 2020).

- For each category from COCO / MVD, which is not merged with any OID leaf-node category in the RVC official taxonomy, HCLS searches all the superclasses from OID and performs one of the following adaptations to the loss:

(a) [Label duplication] Suppose this category matches one of the superclasses from OID in semantics. In this case, HCLS ignores the loss between its OID equivalent and itself, in addition to the losses between its OID equivalent's parents/children and itself.

(b) [Cross-dataset semantic hierarchy] Suppose this category belongs to one of the superclasses from OID in semantics. HCLS ignores the losses between all its parent categories and itself.

(c) [Neither] Suppose this category is independent of any superclass of OID. HCLS does nothing about loss adaptation. In other words, we equally calculate losses over all the categories in the unified label space in loss functions.

In Fig. 2 and Fig. 3, two examples illustrate the loss adaptation process: (a) and (b). Note that we do **not** perform any tedious category merging but rather handle label duplication at the loss level. According to the RVC official taxonomy, there are less than 50 independent categories, so we manually search for cross-dataset label duplication and semantic hierarchy. For further details, please refer to Table 1, which lists the processed semantically duplicate categories, and Table 2, which lists the processed semantic hierarchies across datasets.

### 3.2.4 Overall Formulation

The overall loss function can be formulated as the weighted sum of the RPN loss and the detector



head loss, described as follows,

$$L = \lambda \cdot L_{rpn} + L_{head} \quad (4)$$

where  $\lambda$  is the weight factor set to 0.7, while  $L_{rpn}$  represents the RPN loss (1) and  $L_{head}$  represents the detector head loss (2). In the detector head loss  $L_{head}$ , the classification loss  $L_{cls}$  is given in (3).

In formulas (1), (2), and (3), the symbols  $p$ ,  $q$ ,  $r$ , and  $x$  denote the respective outputs for RPN regression branch, RPN classification branch, the detector head regression branch, and the detector head classification branch, while the  $y$  denotes the corresponding ground truth.  $N$  is the number of samples in each mini-batch.  $C$  is the number of categories including *background* in the unified label space.  $S_{rpn}$  represents the number of stages of Cascade RPN while  $S_{head}$  represents the number of stages of Cascade R-CNN. We set  $S_{rpn}$  to 2 and  $S_{head}$  to 3 for a performance-cost trade-off reason.  $IoU$  represents the IoU loss (Yu, Jiang, Wang, Cao, & Huang, 2016),  $BCE$  represents the binary cross entropy loss, and  $SmoothL_1$  represents the smooth L1 loss.  $\mathbb{1}_{\mathbb{A}}(x)$  represents the indicator function in which the result turns out 1 when  $x \in \mathbb{A}$ . Specifically,  $\mathbb{D}(y)$  denotes the union of the categories involved in HCLS for class  $y$ , as described in Section 3.2.3.  $\mathbb{P}(y)$  denotes the union of the parent categories of class  $y$  as described in Section 3.2.2. The loss weights  $\alpha$ ,  $\beta$ , and  $\gamma$  are set to 10.0, 1.0, and 1.5, respectively.

## 4 Experiments

### 4.1 Datasets

Table 3 provides a brief overview of the three datasets used in the experiments. The COCO dataset (T.-Y. Lin et al., 2014) consists of everyday images of objects and humans, annotated with 80 common object categories. The MVD dataset (Neuhof, Ollmann, Rota Buló, & Kontschieder, 2017) is a high-resolution street-scene imagery dataset, and version 1.2 is used in the experiments, including 37 object categories. Unlike COCO and MVD, the OID dataset (Kuznetsova et al., 2020) is annotated with a semantic hierarchy, and the images are diverse, often containing multiple objects and complex scenes. The annotated classes have a long-tailed distribution, and the training set with

Dataset	Domain	# Cats	# Imgs
COCO	Internet images	80	118k
MVD	Street scenes	37	1.8k
OID	Internet images	500	1.8M

**Table 3** The training datasets used in the experiments, which are provided by organizers of RVC 2022.

500 object categories is used, following the standard practice of Open Images Challenge 2019.

### 4.2 Implementation Details

For our experiments, we adopt the mmdetection codebase (Chen et al., 2019) for the implementation of the proposed method. Our method uses the frozen SEER-RegNet32gf and SEER-RegNet256gf as the backbone, providing a resource-efficient training formulation. In order to ensure synchronous computation across all GPU workers, we replace the traditional BatchNorm (BN) with synchronized BatchNorm (SyncBN). The hyperparameters for the NAS-FPN, Cascade RPN, and Cascade R-CNN components are kept as default, unless specified otherwise.

We employ standard data augmentation techniques such as random flipping and random scaling of the short edge of the image within a range of [480, 960]. The optimization process is conducted using the Stochastic Gradient Descent (SGD) optimizer, with a base learning rate of 0.01, a weight decay of 0.0001, and a batch size of 16. To address the imbalanced class distribution and size disparities across the three datasets, we adopt both class-aware sampling and dataset-wise re-sampling. The re-sampling ratio is set to 1: 4: 8 for OID, COCO, and MVD, respectively. The model training is performed on 8 NVIDIA 3090 / A100 GPUs, with the mixed-precision technique (Micikevicius et al., 2018) being used to speed up the process. During the inference stage, the short edge of the images is resized to 800 while the long edge is restricted to 1333, keeping the aspect ratio unchanged, unless specified otherwise.

### 4.3 RVC Submission

Our RVC final submission utilized a modified version of the proposed detector based on SEER-RegNet256gf. To meet the RVC deadline, certain simplifications were made to the model:

Methods	COCO <i>test</i>		COCO <i>val</i>		MVD <i>test</i>		MVD <i>val</i>		OID <i>test</i>	OID <i>val</i>
	mAP	AP50	mAP	AP50	mAP	AP50	mAP	AP50	AP50	AP50
MD_RVC (1)	59.0	76.0	-	-	32.8	49.3	-	-	62.1	-
IFFF_RVC (2)	50.0	69.0	50.0	69.1	25.3	39.0	24.2	38.6	59.9	69.1
USTC_RVC (3)	50.0	68.0	-	-	25.1	37.9	-	-	47.8	-
CBS_RVC (4)	48.0	66.0	-	-	13.5	21.5	-	-	47.7	-
TSDREF_RVC (5)	19.0	31.0	-	-	6.6	11.6	-	-	40.2	-
Large-UniDet [S]	-	-	48.8	66.2	-	-	25.9	39.4	-	68.5
Large-UniDet [L]	-	-	<b>51.9</b>	<b>70.0</b>	-	-	<b>27.7</b>	<b>42.2</b>	-	<b>69.8</b>
Large-UniDet [S] <sup>†</sup>	-	-	52.0	70.4	-	-	32.0	47.8	-	69.2
Large-UniDet [L] <sup>†</sup>	-	-	<b>53.5</b>	<b>71.8</b>	-	-	<b>33.2</b>	<b>49.4</b>	-	<b>70.5</b>

**Table 4** Comparisons on five RVC submissions on three datasets, the numbers in brackets denote the achieved places in the challenge. The last four rows report our new results in this paper, we only provide the accuracy on validation sets as the RVC test server is off after RVC deadline. Large-UniDet [S] indicates our method based on SEER-RegNet32gf while Large-UniDet [L] indicates the one based on SEER-RegNet256gf. The training of both [S] and [L] starts with the base learning rate of 0.01, which is warm-uped in the preceding 4k iterations and is decreased by a factor of 10 at 850k and 1.0M iterations, and stop at 1.15M iterations. Additionally, the following finetune detailed in Section 4.5.4 is conducted, whose results are distinguished by superscript <sup>†</sup>.

- Instead of using the default setting of  $\{C_2, C_3, C_4, C_5\}$  in NAS-FPN, the side-outputs  $\{C_3, C_4, C_5\}$  were employed and a  $2\times$  downsampling was performed on  $C_5$  twice to create a 5-level feature pyramid. Although this simplification reduced the accuracy of detecting small objects, it significantly shortened the training time.
- The basic anchor scale in Cascade RPN was decreased to 5.04 ( $4 \times 2^{1/3}$ ) to align with the changes in NAS-FPN and to reduce missed detections of small objects.
- The model was trained for 720,000 iterations, with the learning rate dropped by a factor of 0.1 at 600,000 iterations.

During the dataset-agnostic inference procedure, the Soft-NMS (Bodla, Singh, Chellappa, & Davis, 2017) was performed with an IoU threshold of 0.6 and a score threshold of 0.001, then,

- for COCO, the max number of predictions per image was restricted to 100, the short edge of the input image was resized to 800.
- for MVD, the max number of predictions per image was restricted to 300, the short edge of the input image was resized to 2048.
- for OID, the max number of predictions per image was restricted to 300, the short edge of the input image was resized to 800.

We did **not** utilize any advanced inference technique, such as multi-scale test augmentation. The performance of our submission (IFFF\_RVC) on the three datasets is summarized in Table 4. For comparison with the results presented in this paper, we evaluate the model for our RVC submission on the validation sets with a maximum of 300 predictions per image, using the standard Non-Maximum Suppression (NMS) method. All other testing configurations are maintained as those used on the test sets.

## 4.4 Main Results

Comparisons on the RVC final submissions, as well as our new results, are summarized in Table 4. The ranked #1 MD\_RVC employs a large transformer-based object detector (Carion et al., 2020) with an acceleration training strategy that increases the input size progressively. From another perspective, our method, named Large-UniDet, is devoted to building a computation & memory-saving training formulation and generating robust multi-domain object detection predictions by taking advantage of large pre-trained vision models.

Compared to our RVC submission IFFF\_RVC, Large-UniDet isn't simplified as the description in Section 4.3 and is further improved with a training practice where the model is adapted for the high resolution of input data (detailed in Section 4.5.4).

Model	mAP	Time (h)
Faster R-CNN	29.0	12
Cascade R-CNN	39.9	13
+ PAFPN	40.8 (+0.9)	16 (+3)
+ Cascade RPN	42.0 (+2.1)	19 (+6)
+ BiFPN ( $\times 1$ )	40.5 (+0.6)	16 (+3)
+ BiFPN ( $\times 3$ )	41.5 (+1.6)	18 (+5)
+ BiFPN ( $\times 5$ )	41.3 (+1.4)	20 (+7)
+ BiFPN ( $\times 7$ )	41.1 (+1.2)	22 (+9)
+ Cascade RPN	42.1 (+2.2)	25 (+12)
+ NAS-FPN ( $\times 1$ )	41.6 (+1.7)	16 (+3)
+ NAS-FPN ( $\times 3$ )	44.2 (+4.3)	18 (+5)
+ NAS-FPN ( $\times 5$ )	45.3 (+5.4)	20 (+7)
+ NAS-FPN ( $\times 7$ )	45.7 (+5.8)	22 (+9)
+ Cascade RPN	47.6 (+7.7)	24 (+11)

**Table 5** Ablation analysis of detector components on COCO *val* set. The models are trained for 12 epochs on 8 NVIDIA 3090 GPUs, with a base learning rate 0.01 which is divided by 10 after 8 and 11 epochs.

As we can see in Table 4, based on a lighter backbone (SEER-RegNet32gf), Large-UniDet achieves 48.8, 66.2, 25.9, 39.4, and 68.5 points in terms of mAP on COCO *val* set, AP50 on COCO *val* set, mAP on MVD *val* set, AP50 on MVD *val* set, and AP50 on OID *val* set, respectively. The larger backbone (SEER-RegNet256gf) improves universal object detection in performance consistently (+3.1 mAP / 3.8 AP50 on COCO, +1.8 mAP / 2.8 AP50 on MVD, +1.3 AP50 on OID), which does demonstrate the effectiveness of visual representations generated by larger vision models. Without the simplifications in our RVC submission, Large-UniDet [S] and [L] are trained for 1.15M iterations, longer than the IFFF\_RVC, with the base learning rate which is linearly warm-upped in the preceding 4k iterations and decreased by a factor of 10 at 850k and 1.0M iterations. When testing, we generate no more than 300 predictions per image with the common NMS for a fair comparison with the IFFF\_RVC on validation sets.

After the universal object detection training, we conduct the dataset-specific individual fine-tuning with the high-resolution training images, detailed in Section 4.5.4. This practice can further improve the performance of three datasets, especially on MVD, which has fairly different characteristics compared with the other two datasets.

Model	mAP	Time (h)
Faster R-CNN	12.8	1.8
Cascade R-CNN	15.2	2.0
+ PAFPN	16.7 (+1.5)	2.5 (+0.5)
+ Cascade RPN	17.3 (+2.1)	3.5 (+1.5)
+ BiFPN ( $\times 1$ )	17.0 (+1.8)	2.5 (+0.5)
+ BiFPN ( $\times 3$ )	17.1 (+1.9)	2.8 (+0.8)
+ BiFPN ( $\times 5$ )	16.8 (+1.6)	3.1 (+1.1)
+ BiFPN ( $\times 7$ )	16.5 (+1.3)	3.4 (+1.4)
+ Cascade RPN	16.7 (+1.5)	4.3 (+2.3)
+ NAS-FPN ( $\times 1$ )	17.3 (+2.1)	2.8 (+0.8)
+ NAS-FPN ( $\times 3$ )	18.3 (+3.1)	3.0 (+1.0)
+ NAS-FPN ( $\times 5$ )	18.6 (+3.4)	3.2 (+1.2)
+ NAS-FPN ( $\times 7$ )	19.4 (+4.2)	3.5 (+1.5)
+ Cascade RPN	20.2 (+5.0)	4.2 (+2.2)

**Table 6** Ablation analysis of detector components on MVD *val* set. For fast convergence, we initialize the models with the counterparts in Table 5, and train them for 12 epochs on 8 NVIDIA 3090 GPUs, with a base learning rate 0.01 which is divided by 10 after 8 and 11 epochs.

The detailed AP numbers are shown in Table 4, denoted as Large-UniDet with superscript <sup>†</sup>.

## 4.5 Ablation Study

### 4.5.1 Detector Components Analysis

We conduct the ablation analysis based on SEER-RegNet32gf. Table 5 and Table 6 report accuracy-cost comparisons about different detector configurations on COCO and MVD, respectively. With a frozen backbone, Cascade R-CNN outperforms the baseline Faster R-CNN by a significant margin, improving the mAP to 39.9 on COCO while 15.2 on MVD with a little increased training cost (+1 hour for COCO and +0.2 hour for MVD).

When integrating the high-capacity necks into Cascade R-CNN, we achieve higher accuracy but simultaneously suffer the increasing computation burden. Three frequently used FPNs are compared in Tables 5 and 6. As we can see, PAFPN (S. Liu et al., 2018) yields 0.9 and 1.5 points improvement, and BiFPN (Tan et al., 2020) yields at most 1.6 and 1.9 points improvement on COCO and MVD, respectively. As a better choice, NAS-FPN yields 5.8 and 4.2 points improvement. Tables 5 and 6 show that the computational cost increases with the number of stacked neck blocks. At the same

Loss Strategy	COCO	MVD	OID
Baseline	36.2	<u>14.4</u>	61.7
Naive loss suppression	<u>36.4</u>	<b>14.5</b>	62.7
Unified hierarchy	36.3	14.0	<u>64.8</u>
OID hierarchy	<u>36.4</u>	14.0	<u>64.8</u>
+ HCLS	<b>37.1</b>	14.3	<b>65.2</b>

**Table 7** Comparison on loss strategies. The used object detector is Cascade R-CNN based on SEER-RegNet32gf. The five models are trained for 420k iterations, with a base learning rate 0.01 which is decayed by a factor of 0.1 at 280k iterations. Note that the metric of COCO and MVD is mAP and the metric of OID is AP50. The best and the second best results are highlighted in **bold font** and under line, respectively.

time, the performance growth is gradually decelerated, and even the performance degrades for the stacked BiFPN. Consequently, we equip our detector with seven stacked NAS-FPN blocks, enjoying a good trade-off between accuracy and cost.

Besides, Cascade RPN brings a consistent gain (+1.0 mAP at least on COCO and +0.2 mAP at least on MVD) across whatever necks, especially for NAS-FPN, without increasing too much extra computational cost.

#### 4.5.2 Hierarchical Loss Strategies

To demonstrate the effectiveness of our hierarchy-aware cross-dataset loss suppression (HCLS), we compare a number of hierarchical loss strategies in Table 7 and Table 8.

- *Baseline* refers to a situation where the semantic hierarchy is not taken into consideration, and each annotated bounding box is assigned a single positive class label. As a result, there is no loss adaptation applied.
- *Naive loss suppression* denotes that the loss calculation for the classification task takes the semantic hierarchy of OID into account by ignoring the losses for the children and parent categories. This approach incorporates the semantic hierarchy by removing the impact of relationships between parent and child categories, but also leads to a loss of positive samples for the superclasses in OID, resulting in lower performance on OID.
- *Unified hierarchy* takes into account all parent-child relationships across datasets by considering the cross-dataset label duplication presented

Loss Strategy	COCO	MVD	OID
Baseline	44.1	<u>17.2</u>	65.3
Naive loss suppression	<b>44.3</b>	<b>17.8</b>	66.2
Unified hierarchy	43.1	17.1	67.1
OID hierarchy	43.5	16.2	67.6
+ HCLS	<u>44.2</u>	<u>17.2</u>	<b>68.0</b>

**Table 8** Comparison on loss strategies. The used object detector is Cascade R-CNN based on SEER-RegNet32gf with NAS-FPN and Cascade RPN. The five models are trained for 420k iterations, with a base learning rate 0.01 which is decayed by a factor of 0.1 at 280k iterations. Note that the metric of COCO and MVD is mAP and the metric of OID is AP50. The best and the second best results are highlighted in **bold font** and under line, respectively.

in Table 1, cross-dataset semantic hierarchy presented in Table 2, and the original semantic hierarchy of OID for each category in the unified label space. It considers all parents and semantic equivalents as positive and eliminates the losses over all child categories, thereby increasing the training set for superclasses with more positive samples, resulting in a significant improvement in performance on OID (+3.1 AP50 in Table 7 and +1.8 AP50 in Table 8). However, this approach may negatively impact the performance on COCO and MVD, as categories from different datasets may match based on language cues, but still be semantically different. For example, the *bear* category in COCO encompasses a wide range of carnivorous mammals of the Ursidae family, while its equivalent *bear* (/m/01dws) in OID includes not only these conventional bears but also *teddy bears* (/m/0kmg4), leading to taxonomy inconsistencies. This was observed in the severe performance decline of the *bear* category in COCO, with an AP of 41.5 using the *Unified hierarchy*, compared to APs over 65.1 for other categories in Table 7, with the best AP of 67.9 achieved by the HCLS.

- *OID hierarchy* only takes into account the semantic hierarchy of OID. It does not consider the relationships between categories from different datasets. This is a common approach when working with OID (X. Zhou et al., 2022), but it means that cross-dataset relationships are not incorporated into the loss adaptation.

Dataset	Backbone	Strategy	mAP	AP50	epochs	Time	Memory
COCO	SEER-RegNet32gf	finetune	50.7	68.8	45	167	16
		freeze	50.9 (+0.2)	69.2 (+0.4)	72	160	10 (-6)
		finetune	49.9	68.3	64	238	16
		freeze	51.4 (+1.5)	69.8 (+1.5)	108	240	10 (-6)
MVD	SEER-RegNet32gf	finetune	23.9	37.7	48	30	16
		freeze	24.1 (+0.2)	38.0 (+0.3)	80	30	10 (-6)
		finetune	24.4	38.2	100	61	16
		freeze	24.8 (+0.4)	39.1 (+0.9)	160	60	10 (-6)
	SEER-RegNet256gf	finetune	25.8	40.4	60	70	60
		freeze	26.0 (+0.2)	40.9 (+0.5)	120	72	15 (-45)

**Table 9** The object detectors are Cascade R-CNN enhanced with NAS-FPN ( $\times 7$ ) and Cascade RPN. The training time is measured in hours and the GPU memory consumption is measured in GB / image. The models are trained with a batch size of 16 on 16 NVIDIA 3090 / A100 GPUs. For comparison purpose, we convert the training time on different devices to the training time on 8 NVIDIA 3090 GPUs uniformly.

- Our loss strategy, denoted as *OID hierarchy + HCLS*, takes into account the semantic hierarchy of OID, label duplication, and semantic hierarchy among the three datasets simultaneously. This loss adaptation approach results in the best AP on OID (+3.5 AP50 in Table 7 and +2.7 AP50 in Table 8), a slight improvement on COCO, and comparable accuracy on MVD compared to the *Baseline*.

#### 4.5.3 Training Strategies

Table 9 compares two training approaches: finetuning the entire object detector, which is denoted as *finetune*, and the approach used in this paper, where the backbone is frozen during training, denoted as *freeze*. We evaluate these two strategies by simultaneously training models on either COCO or MVD, using either the lighter SEER backbone or the larger one, in terms of performance and GPU memory consumption.

##### - Performance

The results of *finetune* and *freeze*, are shown in Table 9. *freeze* consistently improves performance across datasets, especially with a longer training schedule. On the other hand, *finetune* shows a decline in performance on COCO with a longer training schedule. This may be due to the backbone representations drifting away from the original SEER visual representations and over-fitting on the smaller downstream dataset,

which weakens the performance of the object detector on COCO.

##### - GPU memory consumption

As we can see in Table 9, freezing the backbone during the training process requires significantly less GPU memory than finetuning the entire object detector, including the backbone. The SEER-RegNet32gf-based model requires 10 GB of memory per image during the training process with the *freeze* strategy, whereas the *finetune* strategy requires 16 GB of memory per image. Similarly, the SEER-RegNet256gf-based model requires 15 GB of memory per image with the *freeze* strategy, while the *finetune* strategy requires 60 GB of memory per image. As a result, freezing the backbone is a more feasible option for training models on memory-constrained computational resources, such as NVIDIA 3090.

#### 4.5.4 Scaling Up and Finetuning

##### *Scaling up during the inference procedure*

As outlined in Section 4.3, the short edges of MVD images were resized to 2048 during the inference process to improve detection results due to the presence of many small objects in high-resolution images. This scaling up improved the mAP by about 3 points on MVD in our RVC submission and significantly benefited the models in this paper as well. Fig. 4 demonstrates that the



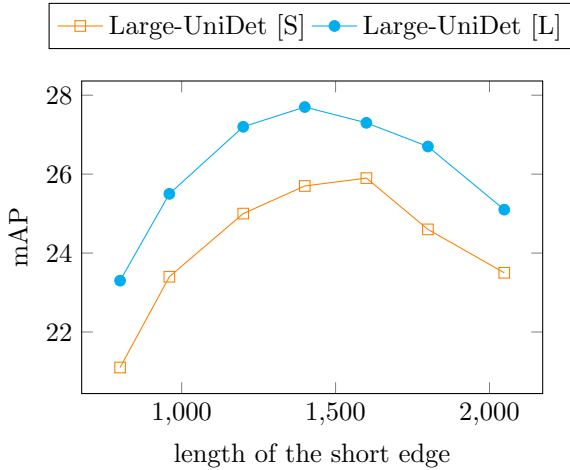


**Fig. 4** The performance on MVD *vs.* the lengths of the short edge of the testing images. We obtain the best mAP at 25.9 with the 1600-pixel resized short edge based on the lighter backbone (Large-UniDet [S]), and obtain best mAP at 27.7 with the 1400-pixel resized short edge based on the larger one (Large-UniDet [L]). The initial mAP and highest mAP of both two models are reported in Table 10.

models obtained through universal object detection training performed best when the short edge of the testing images was resized to 1600 (for Large-UniDet[S]) or 1400 (for Large-UniDet[L]). The best results and the 800-pixel short-edge base-lines can be found in Table 10. Scaling up had a significant impact on MVD for both the small and large models, leading to an increase of +4.8 mAP and +4.4 mAP, respectively.

It is important to note that scaling up the size of the testing images does not result in improved performance on COCO or OID. This is because while the inference scaling improves the detection of small objects, it negatively impacts the performance for larger objects, as previously reported in the literature (Gao, Yu, Li, Morariu, & Davis, 2018). With this in mind, we believe that adapting the object detector for high-resolution images has the potential to improve the detection of large objects while still maintaining the improvement for small objects.

#### *Dataset-specific finetuning with scaling up*

The acceleration practice of training with high-resolution images after low-resolution pre-training can achieve satisfactory performance while reducing the computational cost during the training process (Singh & Davis, 2018). After conducting universal object detection training, we carry out dataset-specific finetuning at a higher resolution,

Model	SU	FT	COCO	MVD	OID
[S]			48.8	21.1	68.5
	✓		-	25.9	-
	✓	✓	<b>52.0</b>	<b>32.0</b>	<b>69.2</b>
[L]			51.9	23.3	69.8
	✓		-	27.7	-
	✓	✓	<b>53.5</b>	<b>33.2</b>	<b>70.5</b>

**Table 10** Comparison on the baseline, scaling up during the inference procedure (denoted as **SU**), and finetuning with higher-resolution training images (denoted as **FT**). The baseline is the universal object detection training without either scaling up the input size when testing or the following dataset-specific high-resolution finetuning. In the table, [S] and [L] represent Large-UniDet [S] and Large-UniDet [L], respectively. The metric of COCO and MVD is mAP and the metric of OID is AP50.

taking into account the performance, training cost, and significant differences among the three datasets.

We use the cosine learning rate annealing with warm restarts (Loshchilov & Hutter, 2016) during the finetuning procedure. Without any alterations to the model design, the finetuning and inference configurations are specified that,

- for COCO, the model is trained for 24 epochs with six cyclical restarts where training images are scaled in a range of [640, 1200] and is evaluated with the 800-pixel resized short edge of testing images;
- for MVD, the model is trained for 24 epochs with six cyclical restarts where training images are scaled in a range of [1024, 2048] and is evaluated with the 2048-pixel resized short edge of testing images;
- for OID, the model is trained for 6 epochs with two cyclical restarts where training images are scaled in a range of [640, 1200] and is evaluated with the 800-pixel resized short edge of testing images.

Table 10 summarizes the results of the finetuning. Based on the lighter backbone, the dataset-specific high-resolution finetuning increases the performance by 3.2 mAP on COCO, 10.9 mAP on MVD, and 0.7 mAP on OID. While based on the larger backbone, the finetuning still retains considerable improvement on three datasets (+1.6 mAP on COCO, +9.9 mAP on MVD, and +0.7 mAP on OID, respectively).

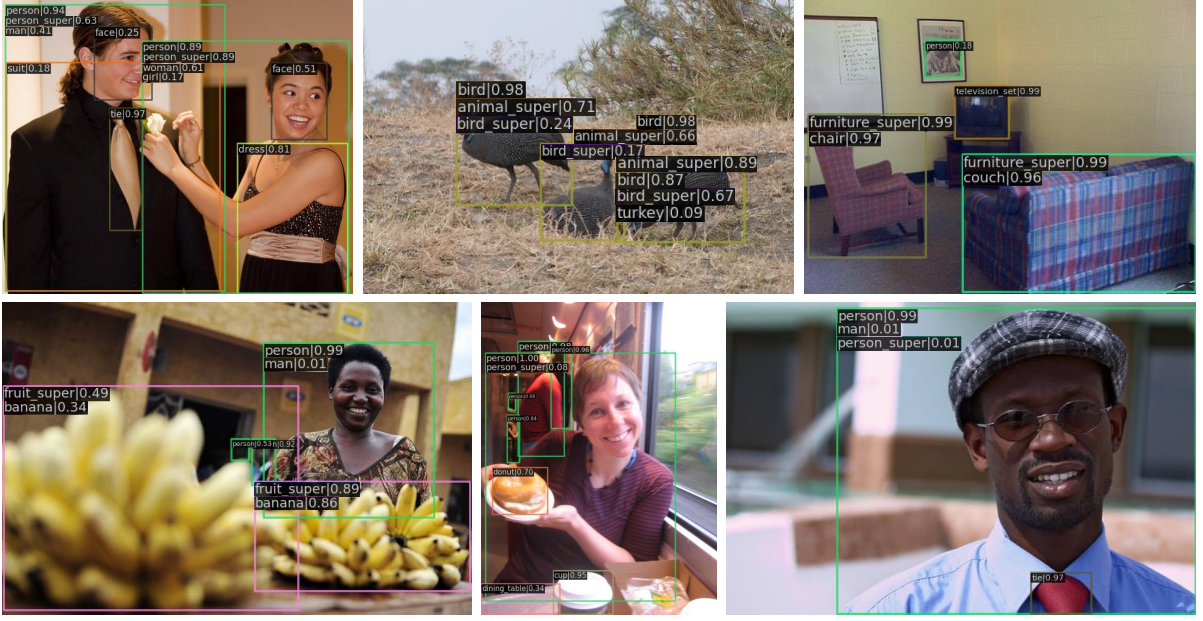


**Fig. 5** Qualitative results on COCO *val* set. On the top left corner of each visualized bounding box, the predicted categories of which the corresponding confidence scores are greater than 0.01 are listed in the descending order of the confidence scores. The entry *classname\_super* indicates this class is a superclass named *classname* in the unified label space.

## 4.6 Visualization

Figs. 5, 6 and 7 showcase the detection results of the Large-UniDet model which uses the SEER-RegNet256gf backbone, and has not undergone further high-resolution specific fine-tuning. These results display up to five recognized categories per bounding box with a confidence threshold, highlighting the presence of category label duplication and semantic hierarchy across datasets in universal object detection. We will delve into this phenomenon in greater detail and provide examples in the subsequent sections.

In the upper-left visualization result in Fig. 5, we can see that a significant number of the categories present in the original label space have been detected successfully. Additionally, some unannotated categories such as *man*, *woman*, *girl*, *person\_super*, *face*, *suit*, and *dress* are also transferred from the other two datasets, despite not being part of the original label space in COCO.

**Label duplication.** The categories *person* and *person\_super* are semantically duplicated, resulting in the high confidence scores for the two people appearing in this image. To be specific, the man is classified as *person* with a confidence score of 0.94 and *person\_super* with a confidence score of 0.63,

meanwhile, the woman is classified as both *person* and *person\_super* with a confidence score of 0.89.

**Semantic hierarchy.** As the categories *woman*, *man*, *girl*, *boy* are subclasses of *person*, the two people in this image are classified as one or more categories among these four subclasses.

**Limitations** In Fig. 5, we can see that while the majority of annotated categories in the original label space of COCO are detected successfully, some unannotated categories are also transferred from the other two datasets. However, the detection and classification of these unannotated categories can be challenging due to annotation inconsistencies across the three datasets. For example, in Fig. 5, the categories *eye*, *nose*, *mouth*, and *hand* from OID are not detected accurately in the COCO images. Additionally, categories such as *person\_super*, *man*, *woman*, and *turkey* that semantically match with objects in COCO images are either detected with low confidence scores or not detected at all. Similarly, Fig. 6 and 7 show similar results for MVD and OID, where categories from other datasets are sometimes omitted.

Given our observations, it appears that our universal object detector is partially overfitting to the unique characteristics of each data domain.



**Fig. 6** Qualitative results on MVD *val* set. On the top left corner of each visualized bounding box, the predicted categories of which the corresponding confidence scores are greater than 0.1 are listed in the descending order of the confidence scores. The entry *classname\_super* indicates this class is a superclass named *classname* in the unified label space.

It seems that the model has discovered a way to “cheat” in universal object detection by memorizing something that distinguishes the testing images from different datasets. This may result in harm to practical applications.

**Discussion** This raises an interesting question - will unifying the annotations in the unified label space improve the performance of the universal object detector on each individual dataset? According to literature (Zhao et al., 2020), the addition of pseudo-labels for unannotated objects has been shown to be effective in the setting of a fully-annotated mixed dataset. However, the impact of annotation inconsistencies on individual datasets has not been thoroughly explored. In Section 4.5.2, we tested a comparable label handling strategy, the *Unified hierarchy*, to unify

the annotations for semantically duplicated categories, but we did not observe any improvement in COCO or MVD as shown in Tables 7 and 8. Despite this, further exploration into this topic is left as open question for future work.

## 5 Conclusion

With the aim of solving the million-scale multi-domain universal object detection problem, we have proposed several resource-efficient techniques for using large vision models to obtain robust visual representations across diverse datasets. Our universal object detector incorporates three essential detector components with high capacity and freezes the parameters of the large vision models. To address the cross-dataset label duplication



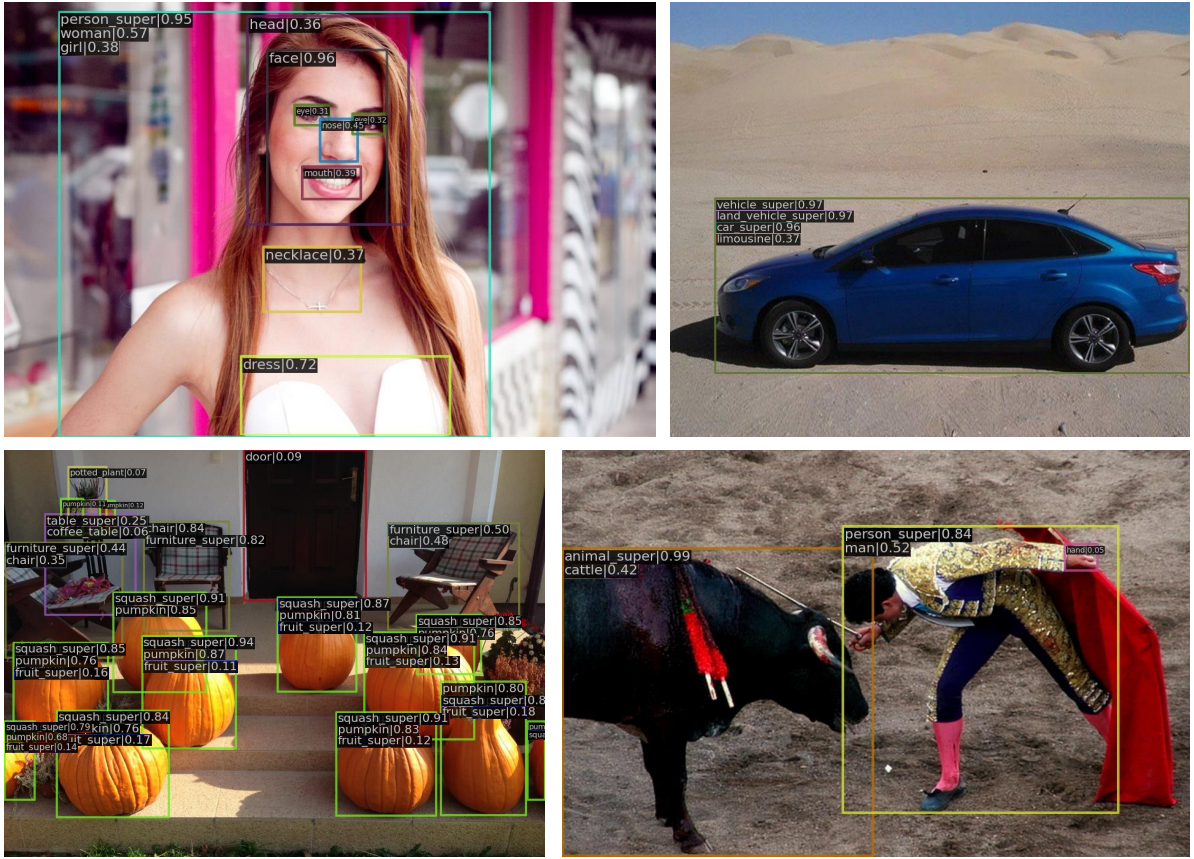


**Fig. 7** Qualitative results on OID *val* set. On the top left corner of each visualized bounding box, the predicted categories of which the corresponding confidence scores are greater than 0.05 are listed in the descending order of the confidence scores. The entry *classname\_super* indicates this class is a superclass named *classname* in the unified label space.

and semantic hierarchy issues, we have implemented hierarchical taxonomy completion and a loss adaptation strategy called hierarchy-aware cross-dataset loss suppression (HCLS) within the unified label space for multiple datasets. Our practices and findings offer a promising solution for real-world computer vision applications and demonstrate the potential for universal object detection.

## Data Availability Statement

The authors confirm the data supporting the findings of this work are available within the article or its supplementary materials.

## References

- Azizi, S., Mustafa, B., Ryan, F., Beaver, Z., Freyberg, J., Deaton, J., ... others (2021). Big self-supervised models advance medical image classification. *Proceedings of the IEEE/CVF international conference on computer vision* (pp. 3478–3488).
- Bello, I., Fedus, W., Du, X., Cubuk, E.D., Srinivas, A., Lin, T.-Y., ... Zoph, B. (2021). Revisiting resnets: Improved training and scaling strategies. *Advances in Neural Information Processing Systems*, 34, 22614–22627.
- Bevandić, P., & Šegvić, S. (2022). Automatic universal taxonomies for multi-domain semantic segmentation. *arXiv*

preprint *arXiv:2207.08445*.

- Bodla, N., Singh, B., Chellappa, R., Davis, L.S. (2017). Soft-nms—improving object detection with one line of code. *Proceedings of the ieee international conference on computer vision* (pp. 5561–5569).
- Bu, X., Peng, J., Yan, J., Tan, T., Zhang, Z. (2021). Gaia: A transfer learning system of object detection that fits your needs. *Proceedings of the ieee/cvf conference on computer vision and pattern recognition* (pp. 274–283).
- Cai, L., Zhang, Z., Zhu, Y., Zhang, L., Li, M., Xue, X. (2022). Bigdetection: A large-scale benchmark for improved object detector pre-training. *Proceedings of the ieee/cvf conference on computer vision and pattern recognition* (pp. 4777–4787).
- Cai, Z., & Vasconcelos, N. (2018). Cascade r-cnn: Delving into high quality object detection. *Proceedings of the ieee conference on computer vision and pattern recognition* (pp. 6154–6162).
- Carion, N., Massa, F., Synnaeve, G., Usunier, N., Kirillov, A., Zagoruyko, S. (2020). End-to-end object detection with transformers. *European conference on computer vision* (pp. 213–229).
- Caron, M., Misra, I., Mairal, J., Goyal, P., Bojanowski, P., Joulin, A. (2020). Unsupervised learning of visual features by contrasting cluster assignments. *Advances in Neural Information Processing Systems*, 33, 9912–9924.
- Chen, K., Wang, J., Pang, J., Cao, Y., Xiong, Y., Li, X., ... others (2019). Mmdetection: Open mmlab detection toolbox and benchmark. *arXiv preprint arXiv:1906.07155*.
- Dai, Z., Liu, H., Le, Q.V., Tan, M. (2021). Coat-net: Marrying convolution and attention for all data sizes. *Advances in Neural Information Processing Systems*, 34, 3965–3977.
- Deng, J., Dong, W., Socher, R., Li, L.-J., Li, K., Fei-Fei, L. (2009). Imagenet: A large-scale hierarchical image database. *2009 ieee conference on computer vision and pattern recognition* (pp. 248–255).
- Devlin, J., Chang, M.-W., Lee, K., Toutanova, K. (2018). Bert: Pre-training of deep bidirectional transformers for language understanding. *arXiv preprint arXiv:1810.04805*.
- Dollar, P., Wojek, C., Schiele, B., Perona, P. (2011). Pedestrian detection: An evaluation of the state of the art. *IEEE transactions on pattern analysis and machine intelligence*, 34(4), 743–761.
- Gao, M., Yu, R., Li, A., Morariu, V.I., Davis, L.S. (2018). Dynamic zoom-in network for fast object detection in large images. *Proceedings of the ieee conference on computer vision and pattern recognition* (pp. 6926–6935).
- Ghiasi, G., Lin, T.-Y., Le, Q.V. (2019). Nas-fpn: Learning scalable feature pyramid architecture for object detection. *Proceedings of the ieee/cvf conference on computer vision and pattern recognition* (pp. 7036–7045).
- Gong, R., Dai, D., Chen, Y., Li, W., Van Gool, L. (2021). mdalu: Multi-source domain adaptation and label unification with partial datasets. *Proceedings of the ieee/cvf international conference on computer vision* (pp. 8876–8885).
- Goyal, P., Duval, Q., Seessel, I., Caron, M., Singh, M., Misra, I., ... Bojanowski, P. (2022). Vision models are more robust and fair when pretrained on uncured images without supervision. *arXiv preprint arXiv:2202.08360*.
- Gupta, A., Dollar, P., Girshick, R. (2019). Lvis: A dataset for large vocabulary instance



- segmentation. *Proceedings of the ieee/cvf conference on computer vision and pattern recognition* (pp. 5356–5364).
- Hasan, I., Liao, S., Li, J., Akram, S.U., Shao, L. (2021). Generalizable pedestrian detection: The elephant in the room. *Proceedings of the ieee/cvf conference on computer vision and pattern recognition* (pp. 11328–11337).
- He, K., Chen, X., Xie, S., Li, Y., Dollár, P., Girshick, R. (2022). Masked autoencoders are scalable vision learners. *Proceedings of the ieee/cvf conference on computer vision and pattern recognition* (pp. 16000–16009).
- He, K., Fan, H., Wu, Y., Xie, S., Girshick, R. (2020). Momentum contrast for unsupervised visual representation learning. *Proceedings of the ieee/cvf conference on computer vision and pattern recognition* (pp. 9729–9738).
- He, Y., Huang, G., Chen, S., Teng, J., Wang, K., Yin, Z., ... Shao, J. (2022). X-learner: Learning cross sources and tasks for universal visual representation. *European conference on computer vision* (pp. 509–528).
- Huang, J., Rathod, V., Sun, C., Zhu, M., Korattikara, A., Fathi, A., ... others (2017). Speed/accuracy trade-offs for modern convolutional object detectors. *Proceedings of the ieee conference on computer vision and pattern recognition* (pp. 7310–7311).
- Jia, C., Yang, Y., Xia, Y., Chen, Y.-T., Parekh, Z., Pham, H., ... Duerig, T. (2021). Scaling up visual and vision-language representation learning with noisy text supervision. *International conference on machine learning* (pp. 4904–4916).
- Joulin, A., Maaten, L.v.d., Jabri, A., Vasilache, N. (2016). Learning visual features from large weakly supervised data. *European conference on computer vision* (pp. 67–84).
- Kolesnikov, A., Zhai, X., Beyer, L. (2019). Revisiting self-supervised visual representation learning. *Proceedings of the ieee/cvf conference on computer vision and pattern recognition* (pp. 1920–1929).
- Kornblith, S., Shlens, J., Le, Q.V. (2019). Do better imagenet models transfer better? *Proceedings of the ieee/cvf conference on computer vision and pattern recognition* (pp. 2661–2671).
- Krishna, R., Zhu, Y., Groth, O., Johnson, J., Hata, K., Kravitz, J., ... others (2017). Visual genome: Connecting language and vision using crowdsourced dense image annotations. *International journal of computer vision*, 123(1), 32–73.
- Kuznetsova, A., Rom, H., Alldrin, N., Uijlings, J., Krasin, I., Pont-Tuset, J., ... others (2020). The open images dataset v4. *International Journal of Computer Vision*, 128(7), 1956–1981.
- Lambert, J., Liu, Z., Sener, O., Hays, J., Koltun, V. (2020). Mseg: A composite dataset for multi-domain semantic segmentation. *Proceedings of the ieee/cvf conference on computer vision and pattern recognition* (pp. 2879–2888).
- Lin, F., Xu, H., Li, H., Xiong, H., Qi, G.-J. (2021). Auto-encoding transformations in reparameterized lie groups for unsupervised learning. *Proceedings of the aaai conference on artificial intelligence* (Vol. 35, pp. 8610–8617).
- Lin, T.-Y., Dollár, P., Girshick, R., He, K., Hariharan, B., Belongie, S. (2017). Feature pyramid networks for object detection. *Proceedings of the ieee conference on computer vision and pattern recognition* (pp. 2117–2125).
- Lin, T.-Y., Maire, M., Belongie, S., Hays, J., Perona, P., Ramanan, D., ... Zitnick, C.L. (2014). Microsoft coco: Common objects in context. *European conference on computer vision* (pp. 740–755).

- Liu, S., Qi, L., Qin, H., Shi, J., Jia, J. (2018). Path aggregation network for instance segmentation. *Proceedings of the ieee conference on computer vision and pattern recognition* (pp. 8759–8768).
- Liu, Y., Wang, Y., Wang, S., Liang, T., Zhao, Q., Tang, Z., Ling, H. (2020). Cbnet: A novel composite backbone network architecture for object detection. *Proceedings of the aaai conference on artificial intelligence* (Vol. 34, pp. 11653–11660).
- Liu, Z., Hu, H., Lin, Y., Yao, Z., Xie, Z., Wei, Y., ... others (2022). Swin transformer v2: Scaling up capacity and resolution. *Proceedings of the ieee/cvf conference on computer vision and pattern recognition* (pp. 12009–12019).
- Loshchilov, I., & Hutter, F. (2016). Sgdr: Stochastic gradient descent with warm restarts. *arXiv preprint arXiv:1608.03983*.
- Meng, L., Dai, X., Chen, Y., Zhang, P., Chen, D., Liu, M., ... Jiang, Y.-G. (2022). Detection hub: Unifying object detection datasets via query adaptation on language embedding. *arXiv preprint arXiv:2206.03484*.
- Micikevicius, P., Narang, S., Alben, J., Diamos, G., Elsen, E., Garcia, D., ... others (2018). Mixed precision training. *International conference on learning representations*.
- Neuhold, G., Ollmann, T., Rota Bulò, S., Kotschieder, P. (2017). The mapillary vistas dataset for semantic understanding of street scenes. *Proceedings of the ieee international conference on computer vision* (pp. 4990–4999).
- Pang, J., Chen, K., Shi, J., Feng, H., Ouyang, W., Lin, D. (2019). Libra r-cnn: Towards balanced learning for object detection. *Proceedings of the ieee/cvf conference on computer vision and pattern recognition* (pp. 821–830).
- Radford, A., Kim, J.W., Hallacy, C., Ramesh, A., Goh, G., Agarwal, S., ... others (2021). Learning transferable visual models from natural language supervision. *International conference on machine learning* (pp. 8748–8763).
- Radosavovic, I., Kosaraju, R.P., Girshick, R., He, K., Dollár, P. (2020). Designing network design spaces. *Proceedings of the ieee/cvf conference on computer vision and pattern recognition* (pp. 10428–10436).
- Ranftl, R., Lasinger, K., Hafner, D., Schindler, K., Koltun, V. (2020). Towards robust monocular depth estimation: Mixing datasets for zero-shot cross-dataset transfer. *IEEE transactions on pattern analysis and machine intelligence*.
- Ren, S., He, K., Girshick, R., Sun, J. (2015). Faster r-cnn: Towards real-time object detection with region proposal networks. *Advances in neural information processing systems*, 28.
- Shao, J., Chen, S., Li, Y., Wang, K., Yin, Z., He, Y., ... others (2021). Intern: A new learning paradigm towards general vision. *arXiv preprint arXiv:2111.08687*.
- Shao, S., Li, Z., Zhang, T., Peng, C., Yu, G., Zhang, X., ... Sun, J. (2019). Objects365: A large-scale, high-quality dataset for object detection. *Proceedings of the ieee/cvf international conference on computer vision* (pp. 8430–8439).
- Singh, B., & Davis, L.S. (2018). An analysis of scale invariance in object detection snip. *Proceedings of the ieee conference on computer vision and pattern recognition* (pp. 3578–3587).
- Sun, C., Shrivastava, A., Singh, S., Gupta, A. (2017). Revisiting unreasonable effectiveness of data in deep learning era. *Proceedings of the ieee international conference on computer vision* (pp. 843–852).

- Tan, M., Pang, R., Le, Q.V. (2020). Efficient-det: Scalable and efficient object detection. *Proceedings of the ieee/cvf conference on computer vision and pattern recognition* (pp. 10781–10790).
- Vasconcelos, C., Birodkar, V., Dumoulin, V. (2022). Proper reuse of image classification features improves object detection. *Proceedings of the ieee/cvf conference on computer vision and pattern recognition* (pp. 13628–13637).
- Vu, T., Jang, H., Pham, T.X., Yoo, C. (2019). Cascade rpn: Delving into high-quality region proposal network with adaptive convolution. *Advances in neural information processing systems*, 32.
- Wang, X., Cai, Z., Gao, D., Vasconcelos, N. (2019). Towards universal object detection by domain attention. *Proceedings of the ieee/cvf conference on computer vision and pattern recognition* (pp. 7289–7298).
- Xu, H., Fang, L., Liang, X., Kang, W., Li, Z. (2020). Universal-rcnn: Universal object detector via transferable graph r-cnn. *Proceedings of the aaai conference on artificial intelligence* (Vol. 34, pp. 12492–12499).
- Xu, H., Zhang, X., Li, H., Xie, L., Dai, W., Xiong, H., Tian, Q. (2022). Seed the views: Hierarchical semantic alignment for contrastive representation learning. *IEEE Transactions on Pattern Analysis and Machine Intelligence*.
- Yu, J., Jiang, Y., Wang, Z., Cao, Z., Huang, T. (2016). Unitbox: An advanced object detection network. *Proceedings of the 24th acm international conference on multimedia* (pp. 516–520).
- Yuan, L., Chen, D., Chen, Y.-L., Codella, N., Dai, X., Gao, J., ... others (2021). Florence: A new foundation model for computer vision. *arXiv preprint arXiv:2111.11432*.
- Zhang, S., Benenson, R., Schiele, B. (2017). Citypersons: A diverse dataset for pedestrian detection. *Proceedings of the ieee conference on computer vision and pattern recognition* (pp. 3213–3221).
- Zhao, X., Schuster, S., Sharma, G., Tsai, Y.-H., Chandraker, M., Wu, Y. (2020). Object detection with a unified label space from multiple datasets. *European conference on computer vision* (pp. 178–193).
- Zhou, B., Zhao, H., Puig, X., Fidler, S., Barriuso, A., Torralba, A. (2017). Scene parsing through ade20k dataset. *Proceedings of the ieee conference on computer vision and pattern recognition* (pp. 633–641).
- Zhou, X., Koltun, V., Krähenbühl, P. (2022). Simple multi-dataset detection. *Proceedings of the ieee/cvf conference on computer vision and pattern recognition* (pp. 7571–7580).